The Solution Structure of the Monomeric Copper, Zinc Superoxide Dismutase from *Salmonella enterica*: Structural Insights To Understand the Evolution toward the Dimeric Structure[†]

Mirko Mori,[‡] Beatriz Jiménez,[‡,#] Mario Piccioli,*[,‡] Andrea Battistoni,*[,§,||] and Marco Sette[⊥]

Magnetic Resonance Center (CERM) and Department of Chemistry, University of Florence, 50019 Sesto Fiorentino (FI), Italy, Department of Biology, University of Rome "Tor Vergata", 00133 Rome, Italy, National Institute of Biostructures and Biosystems (INBB), Viale delle Medaglie d'Oro 305, 00136 Rome, Italy, and Department of Chemical Science and Technology, University of Rome "Tor Vergata", 00133 Rome, Italy

Received July 3, 2008; Revised Manuscript Received September 19, 2008

ABSTRACT: The structure of the SodCII-encoded monomeric Cu, Zn superoxide dismutase from *Salmonella enterica* has been solved by NMR spectroscopy. This represents the first solution structure of a natural and fully active monomeric superoxide dismutase in solution, providing information useful for the interpretation of the evolutional development of these enzymes. The protein scaffold consists of the characteristic β-barrel common to the whole enzyme family. The general shape of the protein is quite similar to that of *Escherichia coli* Cu, Zn superoxide dismutase, although some differences are observed mainly in the active site. SodCII presents a more rigid conformation with respect to the engineered monomeric mutants of the human Cu, Zn superoxide dismutase, even though significant disorder is still present in the loops shaping the active site. The analysis of both dynamics and hydration properties of the protein in solution highlights the factors required to maintain the fully active and, at the same time, monomeric protein. This study provides novel insights into the functional differences between monomeric and dimeric bacterial Cu, Zn superoxide dismutases, in turn helping to explain the convergent evolution toward a dimeric structure in prokaryotic and eukaryotic enzymes of this class.

Copper, zinc superoxide dismutases (CuZnSOD hereafter)[1] are a class of enzymes that catalyze the disproportion of superoxide radical into oxygen and hydrogen peroxide. Discovered about 40 years ago, they are among the most extensively characterized metalloenzymes in terms of biophysical properties, structure−function relationships, and biological functions (*1*). They have been isolated and studied from a number of eukaryotic and prokaryotic sources (*2*).

Eukaryotic CuZnSODs isolated so far are homodimeric enzymes with an impressive degree of structural homology (*2*). Upon site-directed mutagenesis, it has been possible to obtain monomeric variants (*3*); however, their activity was invariantly lower than that of the native dimeric enzymes (*4*). The availability of mutants of the human enzyme in the monomeric form has facilitated the acquisition of detailed NMR structures (*5*) that, later on, have been extended also to the dimeric form of yeast and human enzymes (*6*). The comparison between solution and solid state structures has led to a better understanding of structural and dynamics processes providing researchers insight concerning structure implication for neurodegenerative diseases such as FALS (*7*).

Prokaryotic CuZnSODs show a much larger structural variability than eukaryotic enzymes, differing either in the active site organization or in the modes of subunit association (*2*). Moreover, some bacterial variants display differences in amino acid sequences, quaternary structures, arrangements of the active site ligands or other species-specific structural/functional properties (*8*−*11*). Interestingly, prokaryotic enzymes can be isolated as active enzymes either as monomers or as dimers with different subunit interfaces (*11*−*14*). The larger structural variability found in prokaryotic enzymes has been addressed via X-ray crystallography (*11, 13, 15*). It has been shown that the subunit architecture is conserved

[†] CIRMMP is gratefully acknowledged for providing access to the high field instrumentation available at CERM, Florence (Contract MIUR-FIRB n.RBLA032ZM7). B.J. is a Marie Curie Intra European Fellow (Grant MEIF-CT-2005-515039).

* To whom correspondence should be addressed. Prof. Mario Piccioli, CERM and Department of Chemistry, University of Florence, Via L. Sacconi 3, 50019 Sesto Fiorentino, Italy; tel 39 055 4574265; fax 39 055 4574253; e-mail: piccioli@cerm.unifi.it. Prof. Andrea Battistoni, Department of Biology, University of Rome "Tor Vergata", Rome, Italy; tel 390672594372; fax 39 0672594311.

[‡] University of Florence.

[#] Present address: Laboratory of Structural Biology, Centro de Investigación Príncipe Felipe, Avda. Autopista del Saler 16, 46012 Valencia, Spain.

[§] Department of Biology, University of Rome "Tor Vergata".

[||] National Institute of Biostructures and Biosystems (INBB).

[⊥] Department of Chemical Science and Technology, University of Rome "Tor Vergata".

[1] Abbreviations:CuZnSOD, copper, zinc superoxide dismutase; NMR, nuclear magnetic resonance; FALS, familial amyotrophic lateral sclerosis; SodCII, monomeric Cu, Zn superoxide dismutase from *Salmonella enterica SodCII* gene; SodCI, dimeric Cu, Zn superoxide dismutase from *Salmonella enterica SodCI* gene; Tris, tris(hydroxymethyl)aminomethane; EDTA, ethylenediaminetetraacetic acid; NOESY, nuclear Overhauser effect spectroscopy; HSQC, heteronuclear single quantum coherence; PHOGSY, protein hydration observed by gradient spectroscopy; CLEANEX-PM, phase-modulated CLEAN chemical exchange; AMBER, assisted model building with energy refinement; SDS−PAGE, sodium dodecyl sulfate−polyacrylamide gel electrophoresis.

10.1021/bi801252e CCC: $40.75
Published on Web 11/12/2008

independently of the enzyme quaternary structure. However, monomeric and dimeric CuZnSODs differ in biochemical properties such as catalytic activity, metal affinity, thermal stability, and susceptibility to protease digestion (*16, 17*). Studies on the enzyme from *Salmonella enterica* demonstrated the functional nonequivalency of monomeric and dimeric forms (*17*). Several strains of this organism possess two independent genes, *sodCI* and *sodCII*, encoding for a dimeric (SodCI) and a monomeric (SodCII) enzyme, respectively (*17*). Although the two proteins catalyze the same reaction and share the same subunit fold, the *sodCI* and *sodCII* genes are not functionally interchangeable, indicating that the two proteins have distinctive structural or functional properties, which are apparently related to their different quaternary structure (*16, 17*). The structure of SodCI has been solved by X-ray crystallography (*15*), while SodCII has 85% sequence identity with the monomeric *Escherichia coli* CuZnSOD (*12*) (See Supporting Information, Figure S1).

To the best of our knowledge, no detailed structural characterization for prokaryotic CuZnSODs in solution currently exists. Therefore, in this study, we aimed to solve the solution structure of the mature, monomeric CuZnSOD encoded by the *sodCII* gene isolated from *Salmonella enterica* serovar Choleraesuis strain (SodCII, hereafter). Differences between solid state and solution state can be related to functional aspects and can be a precious source of information to understand reactivity (*5, 18*). Moreover, solution state NMR studies provide unique information on local dynamics that might, in turn, explain functional differences between monomeric and dimeric bacterial and eukaryotic CuZnSODs.

Since the presence of a paramagnetic Cu(II) ion would broaden beyond detection NMR signals within a large sphere around the metal center (*19*), we solved the structure of the reduced Cu(I) state of the protein, which is diamagnetic. We used a so-called hybrid NMR approach, in which the recently developed battery of ^{13}C direct detected experiments (*20*) was used together with routine triple resonance ^{1}H detected experiments to assist NMR assignment and structure determination (*21*). The present structure represents one of the first applications of this tool for structural biologists.

MATERIALS AND METHODS

Protein Expression and Purification. The nucleotide sequence encoding SodCII was inserted in the plasmid pSE420 under control of the *trc* promoter, thus obtaining plasmid pSESCSodCII. This was introduced into *Escherichia coli* BL21 cells to overproduce the protein. Bacteria were cultivated in M9 minimal medium supplemented with 1.5 $\times$ 10^{-5} M $ZnSO_4$ and 4 $\times$ 10^{-6} M $CuSO_4$. ^{15}N-labeled and ^{15}N- and ^{13}C-labeled protein samples were obtained by preparing the minimal M9 medium with ^{15}N ammonium chloride and ^{13}C-glucose purchased from Spectra 2000 (Rome, Italy). Protein overexpression was obtained by inducing the transcription from the *trc* promoter in mid-log-phase cultures by the addition of 1 mM isopropyl-β-D-thiogalactopyranoside (IPTG). After 16 h of growth, cells were harvested by centrifugation and resuspended in 20% sucrose, 30 mM Tris-HCl, pH 8.0, 1 mM EDTA. After incubation on ice in the presence of 1 mg/mL lysozyme, bacteria were centrifuged at 12000*g*, and the supernatant was fractionated by $(NH_4)_2SO_4$ precipitation. Fractions containing CuZnSOD were collected, dialyzed against 150 mM NaCl, 20 mM Tris-HCl, pH 7.4, concentrated to a small volume, and then injected onto a HiLoadTM 16/60 SuperdexTM 75 FPLC gel filtration column (GE-Healthcare). Fractions containing the monomeric protein were concentrated, dialyzed against 20 mM Tris-HCl, pH 7.4, and subjected to ion exchange chromatography on a HiLoad 16/60 FPLC column (Pharmacia) using a 0−0.1 M NaCl linear gradient. Fractions containing CuZnSOD were concentrated and dialyzed against 10 mM phosphate buffer, pH 6.0. Enzyme purity was checked by SDS−PAGE gel electrophoresis.

NMR Experiments. All 2D and 3D spectra were collected at 298 K on Bruker Avance 500, 600, 700, 800, and 900 MHz spectrometers, processed using the TOPSPIN software package (Bruker, Switzerland), and analyzed using CARA software (ETH, Zurich, Switzerland). NMR experiments required to obtain the complete assignment of protein resonances have been previously published (*22*) and are summarized in Supporting Information, Table S2, together with the NMR experiments used to obtain NOE intensities and ^{3}J coupling constants: 2D NOESY, ^{15}N- and ^{13}C-HSQC−NOESY, HNHA, and HNHB.

^{15}N longitudinal and transversal relaxation rates (R_1, R_2), as well as ^{1}H−^{15}N NOE values, were measured at 600 MHz, 298 K, as reported in Supporting Information, Table S2. R_1 and R_2 were obtained by fitting peak intensities, measured as a function of the relaxation delay, to a single-exponential decay by using the Levenberg−Marquardt algorithm. Uncertainties had been evaluated by using a Monte Carlo approach. Heteronuclear NOE values were calculated as the ratio of peak intensities in spectra recorded with and without saturation of amide protons. Relaxation data were analyzed using the FASTModelfree software (*23*), which simplifies the input of the Modelfree package.

Hydration properties were studied at 500 MHz via ^{15}N-HSQC−PHOGSY (*24*) and ^{15}N-HSQC−CLEANEX-PM (see Supporting Information, Table S2). All spectrometers, except the 600 MHz spectrometer, were equipped with cryogenically cooled triple resonance ^{1}H probe with a cooled ^{13}C preamplifier (CP-TCI).

Structure Calculation and Refinement. Structure calculation was performed with the software package ATNOS/CANDID/CYANA, using as input the amino acid sequence, the chemical shift lists, and three NMR spectra (two-dimensional NOESY, three-dimensional ^{13}C-resolved NOESY, and three-dimensional ^{15}N-resolved NOESY). The standard protocol was applied using seven cycles of peak picking with ATNOS (*25*), NOE assignment with CANDID (*25*), and structure calculation with CYANA-2.1. Constraints on φ and ψ dihedral angles were derived from the chemical shift index (*26*) and from HNHA, HNHB, and HSQC−NOESY. $^{3}J_{HNH\alpha}$ coupling constants were obtained from the ratio between the intensity of diagonal and cross peaks integrated on ^{1}H−^{1}H slices of the HNHA experiment and taking into account the proper correction factor. Scalar coupling constants were converted into dihedral angle constraints by the established Karplus relationship. The ratio between $H_N(i)$−H$\alpha(i)$ and $H_N(i)$−H$\alpha(i-1)$ NOEs taken from HSQC−NOESY experiments, provided information on ψ dihedral angles. Overall, 138 φ and 131 ψ dihedral angle values were inserted into the calculation with a tolerance of $\pm$30°.

Stereospecific assignments were obtained with the program GLOMSA. In the final run, 112 stereospecific assignments were used for calculations. Hydrogen bonds were derived from long-range HNCO experiments (*27*). Overall, 89 hydrogen bonds were used, with H−O distance limits in the 1.8−2.0 Å range. The chemical shift of the Cys55 Cβ atom is indicative of the presence of a disulfide bridge between Cys55 and Cys150. Therefore, the inter-residue Sγ−Sγ distance was supposed to be in the 2.0−2.1 Å range. In each ATNOS/CANDID cycle, angle constraints were combined with the updated NOE upper distance constraints for the subsequent CYANA-2.1 structure calculation cycle. In the final ATNOS−CANDID−CYANA cycle, we obtained 4454 cross-peaks and 3563 assignments from 2D NOESY, 2430 cross-peaks and 2066 assignments from 3D ^{15}N-resolved NOESY, and 3369 cross-peaks and 2751 assignments from ^{13}C-resolved NOESY. At the end of the CANDID module, we had 3291 NOE constraints. After CYANA structure calculation, we obtained a family of 20 conformers with a target function of 10.29 Å and rmsd of 0.63 Å. Using CYANA-2.1, we inserted metal ions Cu(I) and Zn(II) in structure calculations as additional constraints, and 30 conformers were considered for the final calculations. Metal ions within CYANA calculations are defined following an established procedure (*5*). According to the binding topology established from spectroscopic data, copper and zinc ions were linked to the imidazole nitrogen atoms of the coordinated histidine or to the carboxylate oxygen of Asp93, with the N−metal or O−metal distances defined with lower limits of 1.80 Å and upper limits of 2.10 Å (*5*). The 30 conformers with the lowest residual target function values were subjected to restraints minimization with the AMBER 8.0 program (D. Case, UCSF). NOE and torsion angle constraints were applied with force constants of 50 kcal mol^{-1} Å^{-2} and 30 kcal mol^{-1} rad^{-2}, respectively. Force field parameters and charges of the metal ions and their ligands were the same as those used for restrained energy minimization and dynamics of reduced form of human dimeric protein (*28*). Structure quality was evaluated using the program PROCHECK-NMR and WHATIF. Structure visualization was done with the program MOLMOL (ETH, Zurich, Switzerland). Structure calculations and analysis were performed on a cluster of Linux PCs.

Atomic coordinates were deposited to the RCSB Protein Data Bank, accession number 2k4w.

RESULTS

NMR Spectral Assignment. Throughout this paper, we have used the amino acid numbering of the mature protein in which the first 19 residues have been deleted. Sequence-specific assignment of backbone and side chain resonances (*22*) was obtained using HSQC, HNCA, HNCO, HNCACB, CBCA(CO)NH, HBHA(CO)NH, (H)CCH-TOCSY, and ^{1}H,^{15}N-NOESY−HSQC. In addition to the set of 2D and 3D ^{1}H-detected experiments, we acquired ^{13}C direct detected CACO, CBCACO, CON and CC-COSY experiments (*20, 29*−*31*). They confirmed proline sequential assignments and provided complete resonance assignment of aspartic acid/asparagine and glutamic acid/glutamine side chains and aromatic rings. Even if ^{13}C direct detection is especially useful for partially or completely unfolded proteins (*32*) or for systems affected by exchange broadening effects, CON experiments provide an alternative fingerprint also for a well-folded protein (*22*).

All atoms observed in routine NMR studies have been identified except serine and cysteine Hγ, threonine Hγ1, tyrosine Hγ, lysine Hε2, Nη, and Hη, phenylalanine Hδ2 and Hε2, and arginine Cη, Nγ1, Hγ11, and Hγ12. The overall assignment was 97%. Almost all ^{13}C resonances were assigned (99.7%), and also the score for ^{1}H was high (96.4%). The lower percentage of ^{15}N assignments (89.4%) was due to side chain atoms, especially those of lysine Nη. The assignment of backbone resonances, including Cβ, was 100%. The complete resonance list has been deposited on the BMRB (accession number 15112) (*22*).

The topology of metal bound histidines has been unambiguously determined from the ^{1}H NMR spectrum of the exchangeable histidine imidazole protons and HSQC patterns (Supporting Information, Figure S3) and from NOESY experiments. NOESY cross peaks from histidine side chains to backbone atoms provide the residue specific assignment of side chain imidazole groups and information on the metal binding topology (*3, 33*). His50 and His128 are bound to the metal via Nε2, while His48, His73, His82, and His90 are bound to the metal via Nδ1. His36 and His45 do not bind any metal ion. The comparison with existing CuZnSOD structures suggests that His48, His50, and His128 are bound to Cu^{+}, while His73, His82, and His90 are bound to Zn^{2+}. Even if there is no direct spectroscopic evidence for the existence of an aspartic acid COO^{-}−Zn^{2+} bond, the presence of a conserved aspartic acid at position 93 that is invariantly bound to Zn^{2+} suggests that Asp93 COO^{-} is Zn-bound, as in the active site of all CuZnSODs characterized thus far. Furthermore, the occurrence of a direct COO^{-}−Zn^{2+} bond is supported by a number of inter-residue NOEs experienced by Asp93 Hβ protons. These NOEs indicate that Asp93 side chain is located in the active site, pointing toward the Zn^{2+} ion.

General Description of the Structure. After restrained energy minimization with the AMBER 8.0 program, the final bundle of 30 conformers of SodCII has an average total target function of 0.60 ± 0.08 Å^2 (CYANA units). The rmsd (residues 3−150) from the average structure is 0.96 ± 0.12 Å for the backbone atoms and 1.30 ± 0.12 Å for the heavy atoms. In Table 1, the statistics on constraint violations in the final family and in the average structure are reported, together with selected quality parameters from a PROCHECK-NMR and WHATIF analysis. These data indicate that the solution structure obtained for SodCII is of good quality. According to the Ramachandran plot (Table 1), 95% (3305 residues) of the non-glycine and non-proline residues have φ dihedral angle in allowed regions, 3.0% (105 residues) in the generously allowed regions, and 2% in disallowed regions (70 residues).

The family of structures obtained for SodCII is shown in Figure 1A (backbone and metal ions only). The structure shows the typical CuZnSOD eight-stranded β-barrel Greek key, conserved in all the conformers (β-strands are depicted in violet in Figure 1A, while the seven loops are in pink). Two small antiparallel β-strands for residues 59−60 and 63−64 in loop IV (cyan) and two short α-helices for residues 117−120 and 141−143 (red) are also observed within loop VI and loop VII, respectively. The α-helix from residues 117−120 is also conserved throughout the family, while the

Table 1: Statistical Analysis of the Energy-Minimized Family of Conformers and Mean Structure of SodCII

	Sod-CII (30 structures)	Sod-CII (mean)
rms Violations per Meaningful Distance Constraints (Å)[a]		
intraresidue (339)	0.0104 ± 0.0014	0.0109
sequential (947)	0.0047 ± 0.0015	0.0040
medium range (391)	0.0026 ± 0.0026	0.0000
long range (1285)	0.0048 ± 0.0011	0.0033
Total (3022)	0.0056 ± 0.0008	0.0048
rms Violations per Meaningful Angle Constraints (deg)		
φ (210)	1.40 ± 0.97	2.1957
ψ (213)	1.59 ± 1.15	0.8915
avg no. constraints per residue	21	
Average Number of Violations per Conformer		
φ	1.87 ± 1.17	2
ψ	1.67 ± 0.94	1
NOE violations larger than 0.3 Å	0.000 ± 0.00	0
NOE violations between 0.1 and 0.3 Å	1.5 ± 1.2845	8
Average rmsd to the Mean (Å)[b]		
backbone	0.96 ± 0.12 Å	1.30 ± 0.12 Å
heavy		
Structural Analysis[c]		
% of residues in most favorable regions	70.5	72.4
% of residues in allowed regions	24.5	22.4
% of residues in generously allowed regions	3	2.6
% of residues in disallowed regions	2	2.6
WHAT IF Structure *Z*-Scores[d]		
1st generation packing quality	−3.195	−3.135
2nd generation packing quality	−1.752	−0.745
Ramachandran plot appearance	−3.617	−2.739
χ_1/χ_2 rotamer normality	−2.878	−2.459
backbone conformation	−3.784	−4.848
WHAT IF rms *Z*-Scores[e]		
bond lengths	0.662	0.653
bond angles	1.303	1.253
omega angle restraints	2.011	2.089
side chain planarity	2.004	1.813
improper dihedral distribution	1.068	1.003
inside/outside distribution	0.928	0.913

[a] Calculated over the 30 conformers representing the NMR structure. The mean value and the standard deviation are given. [b] Calculated for the backbone atoms N, Cα, and C′ of residues 3−150. [c] Ramachandran plot analysis performed with PROCHECK. [d] Calculated on all residues with the exception of those located in loop IV. A *Z*-score is defined as the deviation from the average value for this indicator observed in a database of high-resolution crystal structures, expressed in units of the standard deviation of this database-derived average. Typically, *Z*-scores below a value of −3 are considered poor, those below −4 are considered bad [Vriend, G. (1990) J. Mol. Graphics 8]. [e] Values calculated on all residues with the exception of those located in loop IV.

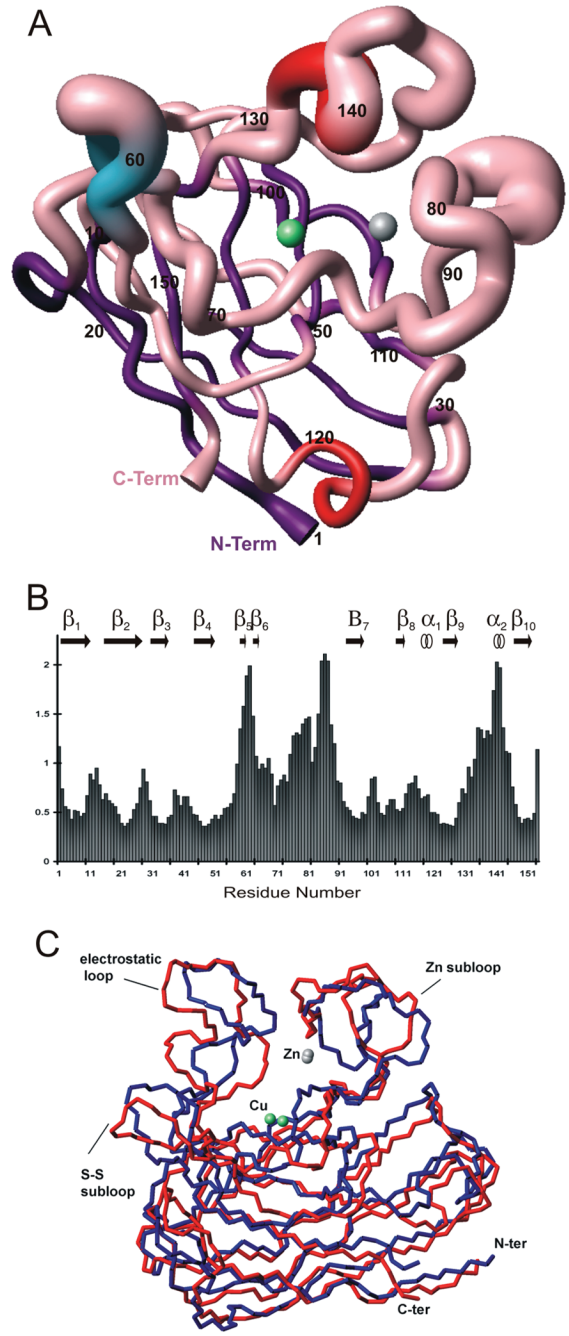

FIGURE 1: (A) Family of 30 accepted structures of reduced SodCII, displayed with MOLMOL. Structures were aligned according to best-fit superimposition of C, Cα, and N atoms of residues 3−150. The metal ions are pictured in green (copper) and in gray (zinc), the β-barrel in purple, the two small β-strands in blue and the two α-helices in red. (B) Backbone rmsd values for the best 30 conformers of SodCII. (C) Superposition of the Cα trace of the mean structure of reduced SodCII (red) with X-ray structure of *E. coli* SOD (blue) (1eso.pdb).

141−143 α-helix is conserved only for 23 out of 30 conformers.

The rmsd for the β-barrel (Figure 1B) is 0.56 ± 0.08 and 1.08 ± 0.0.15 Å for backbone and all heavy atoms, respectively. The most disordered regions, where backbone rmsd exceeds 1 Å, extend from Ala58 to Ala64, from Asp75 to Gly89, and from Gly131 to Gly145. Region 58−64 also includes the two β-strands that do not belong to the β-barrel. Region 75−89, which has the largest rmsd (ca. 2.5 Å), encompasses the Zn bound ligands from His73 to His90. Both regions 58−64 and 75−89 belong to the long loop IV, which, together with loop VI and loop VII, provides the architecture to build the metal binding site and the active cavity. Also the Gly131−Gly145 region is critical for CuZnSODs, because this segment participates in the construction of the active site.

A comparison of the NMR structure of SodCII with the X-ray structure of the *E. coli* enzyme, depicted in Figure 1C, identifies only minor differences in the β-barrel. The topology of loop IV, the longest loop of the enzyme, is well conserved in the two structures. Indeed, the disulfide bridge

between Cys55, at the beginning of loop IV, and Cys150 in strand 8 contribute to anchor loop IV with respect to the β-barrel, therefore favoring the typical loop topology that gives rise to the zinc binding pocket. The short α-helix identified in *E. coli* CuZnSOD between residues 64 and 67 is not apparent in SodCII, where it is instead replaced by two short β-strand segments.

Active Site Channel. Residues that define the access to the active site channel are located in the first part of loop IV, also termed the S−S subloop (residues 51−73), and in loop VII, referred to as the electrostatic loop (residues 129−146) in the eukaryotic enzymes. For all of them, the local backbone rmsd is larger than the average value. As observed in other bacterial CuZnSODs (*14*), these loops display major structural differences with respect to eukaryotic enzymes. In bacteria, the S−S subloop region has an eight-residue insertion, whereas loop VII shows a four-residue deletion. The longer S−S subloop folds at the entrance of the active site channel and contributes to reduce solvent exposure. In SodCII, this loop conserves the charged residue motif (KDGK) typical of most bacterial CuZnSODs (*2*). These residues are located in front of the active site channel and are involved in the electrostatic substrate attraction toward the active site, thus functionally substituting the charged residues located in loop VII in the eukaryotic enzymes (*34*). Unlike the dimeric bacterial enzymes, the S−S loop of SodCII and *E. coli* CuZnSOD contains an additional glutamic acid residue at position 68.

A conserved residue within the electrostatic loop is Arg147 (*2*). This is a key residue for the activity because it is either involved in the electrostatic attraction mechanism or in a direct interaction with the substrate (*3, 5*). The role and the orientation of its guanidinium group has been proposed to be a driving factor for the enzymatic activity (*5*). In human oxidized CuZnSOD (*35*), three H-bonds with neighboring residues locate the side chain of Arg147, while in *Xenopus laevis* CuZnSOD (*36*) the correct orientation is mainly given by hydrophobic interactions between its side chain and neighboring residues. In *E. coli* CuZnSOD, the orientation of Arg147 is imposed by a salt link between its guanidinium group and Glu68 (*37*), and it is thought that this interaction can compensate the absence of other stabilizing contacts that occur in eukaryotic CuZnSODs (*12*). In the present structure, Arg147 is not involved in any H-bond network similar to that characterizing human CuZnSOD (*38*). We observe three residues, Ala66, Met126, and Val10, whose side chains are close to the aliphatic part of Arg147 with inter-residue H−H distances between 3.80 and 4.75 Å. This suggests that hydrophobic interactions among the aliphatic side chain of Arg147 and nearby residues play a major role for the optimal orientation of the arginine residue as previously observed in *X. laevis* CuZnSOD (*2*). From the ensemble of structures, we have found two different conformations for Arg147. One of them is closer to the active site and corresponds to the position present in the average structure, whereas the other one is more solvent-exposed. The average structure suggests an interaction between Arg147 guanidinium groups and Gly145 and Ala67 carbonyl oxygens (147 Nη1−145 O = 2.83 Å; 147 Nη2−67 O = 2.78 Å). A very similar orientation is found in *E. coli* CuZnSOD.

Metal Binding Residues. The average rmsd calculated over metal binding residues, considering all heavy atoms, is smaller than 1 Å, and it is lower than the average global value observed for side chains. Indeed, metal-to-donor coordination bonds and several inter-residue NOEs among histidines contribute to the precision of the active site structure. The superimposition of backbone atoms of the metal ion ligands in SodCII and *E. coli* CuZnSOD, shown in Figure 2, exhibits an rmsd value of 0.47 Å.

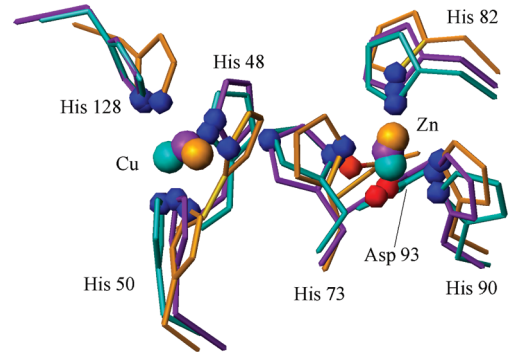

FIGURE 2: The active site superimposition of SodCII (orange), *E. coli* CuZnSOD (purple), and human CuZnSOD (green-blue).

Zn-bound His73 is protonated at the Nε2 position, consistent with a broken bridge and an imidazole ring tilted with respect to the oxidized form. The distance between copper and HNε2 is 3.15 Å, and it is larger than the van der Waals distance, while the distance between the copper ion and His73Nε2 is 3.28 Å. A similar Cu−N distance (3.44 Å) has been observed in the human reduced enzyme solved by NMR (*5*). This is also consistent with the X-ray structure of the fully reduced yeast enzyme, in which the Cu-HisNε2 is 3.2 Å, longer than that observed in oxidized CuZnSODs (2.1 Å in *X. laevis*, for example) (*39*). In contrast, intermediate distances were found in the crystal structure of oxidized bacterial enzymes from *E. coli* (2.7 Å) (*12*) and SodCI (2.5 Å) (*15*). As previously suggested (*40*), in the prokaryotic enzymes solved by X-ray crystallography, a partial but not complete reduction of the copper ion occurred under the X-ray beam.

The oxidation state of the copper ion is possibly responsible for some of the differences observed between SodCII and *E. coli* SOD. Among them, the His73 ring plane flips by approximately 20° with respect to the position occurring in *E. coli* when the bridge between the two metal ions is present. This movement is similar to that previously revealed by NMR in the case of the human enzyme and is required to prevent the occurrence of van der Waals violations when His73 is protonated at the Nε2 position.

A slight shift is also observed for His128, one of the copper ion ligands. In SodCII, the His128 ring plane moves toward His48 with respect to the position observed in the *E. coli* enzyme. As a consequence, the distance between His128 Cε1 and His48 Nδ1 is 3.79 Å, while in *E. coli* CuZnSOD it is 4.29 Å. However, the Cu−Zn distance is 6.6 Å, which is similar to that observed in *E. coli* CuZnSOD (6.5 Å) and in most of the available X-ray and NMR structures of other CuZnSODs (*2*). Even though NMR data do not provide direct constraints on the Cu−Zn distances, and the latter is driven not only by the experimental NMR restraints but also from the additional links imposed from the histidine donor atoms to the metal, these data indicate that the metal−metal distances are not affected by metal ion reduction. Another

Table 2: Interface Residues in PlSod, ApSod, SodCI, SodCII, and *E.coli* Sod[a]

	2,3 loop		β6d	Zn subloop	β5e	β4f		7,8 loop	
	27−29	32	44	84, 85B, 87	96−98	107−110	112, 113	132	134
PlSod	NK**Y**	V	M	FW**D**	A**L**F	N**PVL**	**PR**	**D**	H
ApSod	SA**Y**	V	L	YW**D**	A**L**F	N**PVL**	**PR**	**D**	H
SodCI	TP**Y**	L	I	GY**D**	G**L**V	Y**PLL**	**PR**	**D**	Y
SodCII	TEG	K	E	G − G	VLV	EPVT	PR	D	M
E. coli Sod	TDK	E	E	G − G	ALV	DAVI	PR	D	M

[a] The fully conserved residues in dimeric Sod are in bold. Numbering refers to the SodCII studied in this work. Both SodCII and *E. coli* Sod have a deletion at position 85B.

crucial residue to build the metal binding site is Asp132. This residue drives the orientation of Cu-bound His48 and Zn-bound His82 forming distinct H-bonds with imidazole HNε2 protons, as occurs in other CuZnSODs.

Comparison between SodCII and Dimeric Bacterial CuZnSODs. The overall molecular fold of SodCII is comparable to that of the subunits of the dimeric enzymes from *Salmonella enterica* (SodCI), *Photobacterium leiognathi* (PlSod) (*39*), and *Actinobacillus pleuropneumoniae* (*40*), which display 62%, 55%, and 62% sequence identity, respectively, to SodCII. In these enzymes, the association of the two subunits is mostly promoted by van der Waals interactions and by a minor contribution from hydrogen bonds (*20, 38*).

In particular, five regions are important for dimeric assembly and stabilization of quaternary structure: loop II, Zn subloop, β-strands 4 and 5, and loop VII. These protein fragments are characterized by some evolutionarily invariant residues that are involved in subunit−subunit interaction. Table 2, where residues are numbered according to SodCII sequence, shows residues at the interface that give rise to three clusters of interactions that drive the dimer stabilization. There are substantial differences between SodCI and SodCII. Four tyrosine residues, Tyr29, Tyr85B, Tyr107, and Tyr134, are missing or substituted with non-aromatic residues in SodCII. The Tyr29→Gly mutation, as well as the Tyr85B deletion, severely impair many of the van der Walls hydrophobic contacts between the two subunits of SodCI. In SodCI, the cluster region is disrupted by residues 84 and 85B on one side, and residues 27, 29, 32, and 108−110 on the other. Additionally, the Tyr29→Gly replacement, together with the Asp87→Gly substitution, prevents the formation of a Tyr29−Asp87 H-bond, which has been described as a crucial factor for the subunit association. Likewise, Tyr107→Glu, together with Ile44→Glu substitution, provides a negatively charged region that prevents van der Walls contacts in the second cluster region, defined by residues 44, 98, and 107. Finally, the hydrophobic cavity that normally hosts the buried water molecule bound to three tyrosine residues, is clearly destabilized by the substitution of the Tyr134 by methionine.

A similar situation applies to the other monomeric protein, that is the *E. coli* enzyme, where the same substitutions described above (Tyr29, Tyr85B, Tyr107, Tyr134, Ile44, and Asp87) are observed.

Thus, the replacement of a few hydrophobic residues and the increase of residues with different size and charge throughout the hypothetical intersubunit region give rise to a surface that is nonconducive to the formation of homo- or heterodimeric proteins.

Protein Hydration. The analysis of ePHOGSY and CLEANEX-PM experiments (*24*) shows the occurrence of water molecules interacting with specific protein regions at different exchange rates. Strong CLEANEX-PM peaks are observed for a few amino acids, namely, residues 3, 12, 18, 28, 31, 49, 61, 63, 67, 72, 101, 145, and 146. They point out the protein regions in which H_2O molecules bind to the protein in an exchange regime faster than the rotational correlation time of the protein. As shown in Figure 3, most of these amino acids (8 out of 13) belong to the active channel. They provide the hydrophilic environment contributing to driving superoxide toward the metal ion. The fast exchange rate experienced by these H_2O molecules is required in order to allow the fast diffusion of substrate to the active site.

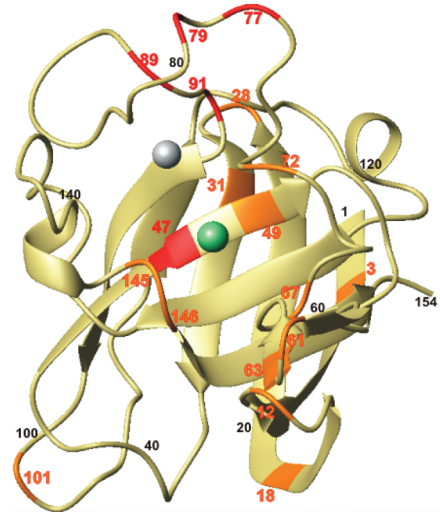

FIGURE 3: SodCII cartoon in which the residues identified via CLEANEX-PM and PHOGSY experiments have been highlighted. Residues colored in yellow (aa 3, 12, 18, 31, 49, 61, 63, 67, 72, 101, 145, and 146) are observed in the CLEANEX-PM experiments. The exchange rate of amide protons with water molecules is faster than the rotational correlation time of the protein. Residues colored in red (aa 47, 77, 79, 89, and 91) are identified via the ePHOGSY experiment. The water−protein interaction is therefore slower than the rotational correlation time (structural water molecule).

The ePHOGSY peak to His48 HNε2 accounts for the presence of a buried water molecule close to the copper ion (*41*). However, the HOH−Cu distance, which is known to be different in various CuZnSODs (*2*), cannot be accurately estimated from this measurement. Another buried water molecule is observed within the Zn-binding loop, indicated by ePHOGSY peaks involving amino acids 77, 79, 89, and 91. However, no ePHOGSY peaks are observed from the Zn-coordinated imidazole NH groups. This suggests that the H_2O molecule observed in proximity of the Zn binding loop is not inside the active cavity. Indeed, residues 75−80 and 85−92 define a loop where a water molecule could be buried due to the presence of H-bonds with Asn78 and Gly89

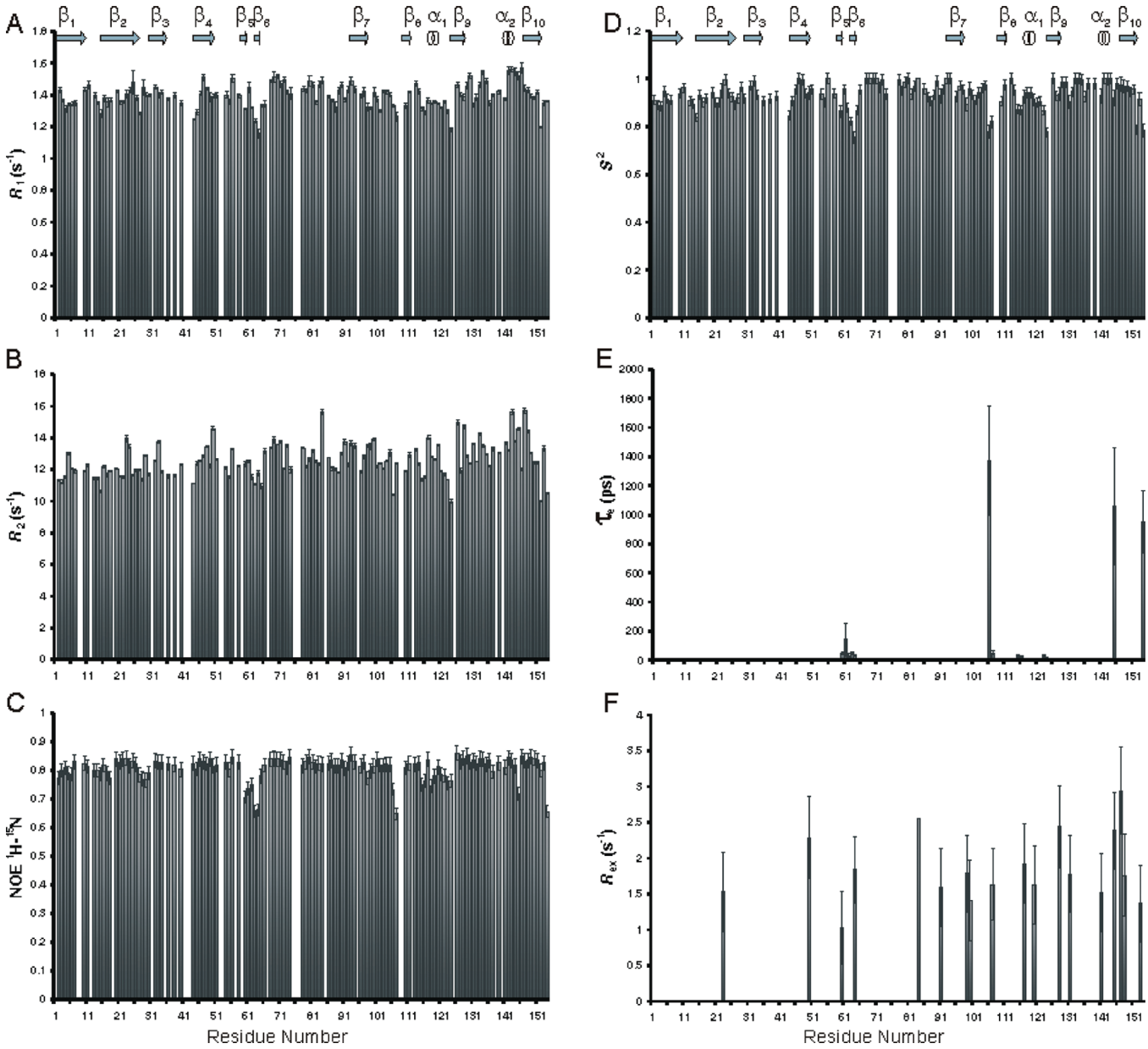

FIGURE 4: Plots showing the relaxation rates and mobility parameters in reduced SodCII, measured at 600 MHz and 298 K: (A) longitudinal relaxation; (B) transverse relaxation; (C) NH NOE; (D) order parameter, S^2; (E) local correlation time for motions on the subnanosecond time scale (τ_s); (F) exchange rates on the millisecond−microsecond time scale (R_{ex}).

contributing to the stabilization of the secondary structure of the Zn-binding loop.

Protein Dynamics in Solution. Relaxation properties of 126 out of 142 assigned $^1H-^{15}N$ resonances were analyzed. Average values of 1.4 ± 0.1 and 12 ± 1 s^{-1} were obtained for ^{15}N longitudinal (R_1) and transverse (R_2) relaxation rates, respectively, while the average $^1H-^{15}N$ NOE value was 0.80 ± 0.04 s^{-1}. A simple isotropic model was sufficient to fit the data using a τ_c of 8.99 ± 0.02 ns. This value is similar to that observed for the monomeric variant of the human superoxide dismutase (*18*), as well as other proteins of its size. The average order parameter value ($S^2 = 0.94 \pm 0.04$) confirms that the protein fold maintains a rigid structure. This value is closest to the dimeric form of the homologous human form ($S^2 = 0.92 \pm 0.09$) compared with that of the monomeric one ($S^2 = 0.89 \pm 0.11$) (*18*), the latter being significantly less active (*5*). Relaxation data for SodCII are summarized in Figure 4. The regions encompassing the two shortest β-sheets in the protein (Ile59−Ala64), the fragment involving Thr106−Glu107, and Ala124 display a faster internal mobility. The two β-sheets in the 58−64 region form a subloop that is quite solvent-exposed (as pointed out by hydration experiments, in which peaks are observed for aa 61 and 63) and that defines the more peripheral part of the active channel. However, low H−N NOEs and small R_2 values suggest that the intervening motions are on the order of subnanoseconds and that no large conformational exchange motions (typically at milli- or microsecond time scale) occur.

DISCUSSION

All the structures of prokaryotic SOD described to date have been obtained via X-ray crystallography. In this frame, the solution structure of SodCII allows us to gain insights into the dynamic and hydration properties of the protein and

to correlate such properties with the enzymatic activity. Recently, it has been observed that the catalytic activity of SodCI is significantly higher than that of SodCII (*17*) and that the activity of SodCII is comparable to that of the monomeric enzyme from *E. coli* (Battistoni et al., manuscript in preparation). The catalytic rate of monomeric *E. coli* and SodCII enzymes, measured by pulse radiolysis at low ionic strength, is about 1.3×10^9 M^{-1} s^{-1} (*34*). This value is comparable to that of the dimeric human enzyme (2.0×10^9 M^{-1} s^{-1}) but is considerably lower than those of the dimeric SodCI (1.3×10^{10} M^{-1} s^{-1}) or PISod (8.5×10^9 M^{-1} s^{-1}) bacterial enzymes (*16*). Moreover, the activity of the natural monomeric prokaryotic enzymes is much higher than those reported for the engineered monomeric human enzymes (about 2.0×10^8 M^{-1} s^{-1}) (*42*) whose large decrease in catalytic rate is a likely consequence of the alterations in the tertiary structure caused by extensive solvation or distortion of the mutated dimer interface.

Our relaxation data allow speculation concerning the activity of the enzyme and the monomer versus the native dimer state. When relaxation data of dimeric vs monomeric mutants of human SOD are compared, motions in the millisecond time scale have been proposed to be responsible of multiple conformations, which eventually prevent the active site residues from assuming a functional orientation (*18*). As no evidence for enhanced local mobility nor conformational exchange on the millisecond time scale is present in SodCII, in contrast to that observed for the partially active monomeric human enzyme, the dynamics of SodCII on the slow time scale resembles the fully active eukaryotic dimeric enzyme rather than the partially active monomeric enzyme. This supports the notion that fluctuations of the electrostatic loop may affect the diffusion of substrate toward the active site and therefore decrease the activity.

The mobility observed on fast time scales for the S−S subloop (see Figure 4) is in excellent agreement with a previous study on the *E. coli* enzyme based on the combined use of limited proteolysis and molecular dynamics, showing that this loop is quite mobile on the nanosecond−picosecond time scale (*43*). The solution structure of dimeric human CuZnSOD reveals an increase in mobility of the loops shaping the active site thus pointing out that subnanosecond mobility facilitates the diffusion of the substrate through the active channel. The solution structure of human CuZnSOD has also revealed that metal ions play a role in protein structure (*44, 45*). Moreover, several studies have suggested that in monomeric bacterial CuZnSODs the mobility of the S−S loop might be affected more than in dimeric ones by metal occupancy of the active site (*17, 46*).

The stability of monomer in solution is favored by the high average S^2 observed. The rigidity of SodCII, together with unfavorable electric charge distribution and the substitution of hydrophobic residues throughout the hypothetical intersubunit region, contributes to the stability of the monomer in solution. It has been already shown that enhanced mobility of those amino acids involved in the subunit−subunit interactions is one of the crucial factors for the aggregation of dimeric CuZnSODs (*7*).

Another relevant result from this work is the identification of water molecules in the active site channel. Thus, the occurrence of increased mobility of the loops shaping the active site and the presence of charged residues important for electrostatic attraction cooperate with the presence of water molecules that can help the diffusion of the substrate in order to obtain high catalytic efficiency.

These observations are relevant to understand the structural and functional differences between monomeric and dimeric enzymes. All characterized eukaryotic CuZnSODs show a tight and stable dimeric structure. The amino acids involved in dimer formation are highly conserved and the subunit−subunit recognition is based both on hydrophobic interactions and direct hydrogen bonding (*5, 13*). The highly conserved dimeric structure, typical of eukaryotic SODs, is not observed in prokaryotic enzymes. Indeed, some enzymes of this class, such as SodCII, are monomeric, while others are dimeric yet present different subunit arrangements (*15*). The residues implicated in the interface subunit in the dimeric prokaryotic enzymes are not always conserved. The surface is much less hydrophobic when compared with the eukaryotic enzymes, and it is characterized by the presence of intervening water molecules, which can be considered components of the bacterial quaternary structure, located within an intersubunit cavity (*2, 14, 15, 47*). Mutations in the interface residues and variations in number and orientation of trapped water molecules may support a fine-tuning of subunit association processes across the different prokaryotic species. Single amino acid mutations at the dimer interface of PlSod significantly decrease the affinity for copper but increase catalytic rates, possibly due to an enhanced copper accessibility and to an altered mobility of the S−S loop (*15, 43*). Species-specific modifications in the intersubunit region have therefore been proposed to contribute also to the exceptionally high activity of SodCI (*15*) and to the differences in dimer stability, metal affinity, and protease resistance between SodCI and PlSod (*16, 17*).

The monomeric enzymes from *E. coli* and *S. enterica* have clearly distinct functional features when compared with the dimeric bacterial enzymes. These include lower activity and thermal stability, looser metal cofactor affinity, and decreased resistance to protease digestion (*16, 17*). These differences have been tentatively explained as a consequence of alterations in the mobility of the loops forming the active site channel. Similar properties have been observed in PlSod interface mutants, which have a strong tendency for monomerization (*2*). The present investigation shows that monomeric SodCII is characterized by significant disorder in the loops shaping the active site, thus supporting this hypothesis.

The dimer interface of prokaryotic and eukaryotic CuZnSODs involves different β-strand elements, indicating an independent evolution toward the dimeric structure (*14*). Comparative studies on naturally occurring monomeric and dimeric bacterial enzymes show that the dimeric structure is associated with higher stability and activity (*16, 17*). This is highlighted by recent studies on the two *Salmonella* enzymes, which have shown that *sodCI* and *sodCII* are not functionally exchangeable (*17*). In fact, when the sequence encoding for SodCII is placed under the control of the *sodCI* promoter, it is not able to complement the lack of *sodCI*, therefore suggesting that the dimeric enzyme has superior properties. This observation raises questions regarding the meaning of monomeric enzymes in different bacteria. Monomers cannot be trivially considered as evolutionary relics still present in the genome of scattered bacteria. In fact, bacteria such as *Salmonella* and *E. coli O157:H7*

express either monomeric or dimeric variants of the enzyme (*48*). Moreover, dimeric CuZnSODs can be isolated from the very ancient hyperthermophilic eubacterium *Aquifex aeolicus* (Battistoni, A., and D'Orazio, M., unpublished observations), indicating that dimeric structure formation in CuZnSOD was an early step during evolution. In fact, SodCI has a clear role in bacterial protection from phagocytic attack (*17*), while the exact role of SodCII is still poorly defined. Although it has been proposed that this enzyme protects bacteria from toxic effects of endogenous superoxide generated within the periplasmic space (*49*), additional studies are required to clarify whether its functions are correlated with the monomeric structure.

In summary, this study describes the first solution structure of a natural monomeric CuZnSOD from *Salmonella enterica*. We provide indications about the mobility and the hydration of the enzyme and clarify the essential factors required to obtain a stable and fully active monomeric enzyme. In addition, the structural and mobility features of the protein surface highlight differences between monomeric and dimeric CuZnSODs, which help to explain the functional diversification between the bacterial enzymes of this class and the convergent evolution of bacterial and eukaryotic CuZnSODs toward the dimeric structure.

ACKNOWLEDGMENT

We thank Prof. I. Bertini and Prof. G. Rotilio for critical reading and continuous support. We acknowledge Dr. F. Cantini for sharing her expertise in CARA and CYANA software. We are grateful to Dr. D. A. MacIntyre for careful readings of this manuscript.

SUPPORTING INFORMATION AVAILABLE

Multiple alignment of amino acid sequence of CuZnSODs, HSQC spectrum of imidazole groups, and acquisition parameters for NMR experiments. This material is available free of charge via the Internet at http://pubs.acs.org.

REFERENCES

1. Valentine, J. S., Doucette, P. A., and Potter, S. Z. (2005) Copper-Zinc Superoxide Dismutase and Amyotrophic Lateral Sclerosis. *Annu. Rev. Biochem. 74*, 563–593.
2. Bordo, D., Pesce, A., Bolognesi, M., Stroppolo, M. E., Falconi, M., and Desideri, A. (2001) *Handbook of Metalloproteins*, pp1284−1300, John Wiley and Sons, Chichester.
3. Bertini, I., Piccioli, M., Viezzoli, M. S., Chiu, C. Y., and Mullenbach, G. T. (1994) A spectroscopic characterization of a monomeric analog of copper-zinc superoxide dismutase. *Eur. J. Biophys. 23*, 167–176.
4. O'Neill, P., Davies, S., Fielden, E. M., Calabrese, L., Capo, C., Marmocchi, F., Natoli, G., and Rotilio, G. (1988) The effects of pH and various salt upon the activity of a series of superoxide dismutases. *Biochem. J. 251*, 41–46.
5. Banci, L., Benedetto, M., Bertini, I., Del Conte, R., Piccioli, M., and Viezzoli, M. S. (1998) Solution structure of reduced monomeric Q133M2 copper, zinc superoxide dismutase. Why is SOD a dimeric enzyme? *Biochemistry 37*, 11780–11791.
6. Banci, L., Bertini, I., Cantini, F., D'Amelio, N., and Gaggelli, E. (2006) Human SOD1 before harboring the catalytic metal: Solution structure of copper-depleted, disulfide-reduced form. *J. Biol. Chem. 281*, 2333–2337.
7. Banci, L., Bertini, I., Girotto, S., Martinelli, M., Vieru, M., Whitelegge, J., Durazo, A., and Valentine, J. S. (2007) Metal-free SOD1 forms amyloid-like oligomers: A possible general mechanism for familial ALS. *Proc. Natl. Acad. Sci. U.S.A. 104*, 11263–11267.
8. Pacello, F., Langford, P. R., Kroll, J. S., Indiani, C., Smulevich, G., Desideri, A., Rotilio, G., and Battistoni, A. (2001) A novel heme protein, the Cu,Zn-superoxide dismutase from *Haemophilus ducreyi*. *J. Biol. Chem. 276*, 30326–30334.
9. Banci, L., Bertini, I., Calderone, V., Cramaro, F., Del Conte, R., Fantoni, A., Mangani, S., Quattrone, A., and Viezzoli, M. S. (2005) A prokaryotic superoxide dismutase paralog lacking two Cu ligands: From largely unstructured in solution to ordered in the crystal. *Proc. Natl. Acad. Sci. U.S.A. 102*, 7541–7546.
10. Battistoni, A., Pacello, F., Mazzetti, A. P., Capo, C., Kroll, J. S., Langford, P. R., Sansone, A., Donnarumma, G., Valenti, P., and Rotilio, G. (2001) A histidine-rich metal binding domain at the N terminus of Cu,Zn-superoxide dismutases from pathogenic bacteria. *J. Biol. Chem. 276*, 30315–30325.
11. Spagnolo, L., Toro, I., D'Orazio, M., O'Neill, P., Pedersen, J. Z., Carugo, O., Rotilio, G., Battistoni, A., and Djinovic-Carugo, K. (2004) Unique features of the sodC-encoded superoxide dismutase from *Mycobacterium tubercolosis*, a fully functional copper-containing enzyme lacking zinc in the active site. *J. Biol. Chem. 279*, 33447–33455.
12. Pesce, A., Capasso, C., Battistoni, A., Folcarelli, S., Rotilio, G., Desideri, A., and Bolognesi, M. (1997) Unique structural features of the monomeric Cu,Zn superoxide dismutase from *Escherichia coli*, revealed by X-ray crystallography. *J. Mol. Biol. 274*, 408–420.
13. Bordo, D., Matak, D., Djinovic-Carugo, K., Rosano, C., Pesce, A., Bolognesi, M., Stroppolo, M. E., Falconi, M., Battistoni, A., and Desideri, A. (1999) Evolutionary constraints for dimer formation in prokaryotic Cu,Zn superoxide dismutase. *J. Mol. Biol. 285*, 283.
14. Bourne, Y., Redford, S. M., Steinman, H. M., Lepock, J. R., Tainer, J. A., and Getzoff, E. D. (1996) Novel dimeric interface and electrostatic recognition in bacterial Cu,Zn superoxide dismutase. *Proc. Natl. Acad. Sci. U.S.A. 93*, 12774–12779.
15. Pesce, A., Battistoni, A., Stroppolo, M. E., Polizio, F., Nardini, M., Kroll, J. S., Langford, P. R., O'Neil, J. D., Sette, M., Desideri, A., and Bolognesi, M. (2000) Functional and crystallographic characterization of *Salmonella typhimurium* Cu,Zn superoxide dismutase coded by the sodCI virulence gene. *J. Mol. Biol. 302*, 465–478.
16. Gabbianelli, R., D'Orazio, M., Pacello, F., O'Neill, P., Nicolini, L., Rotilio, G., and Battistoni, A. (2004) Distinctive functional features in prokaryotic and eukaryotic Cu,Zn superoxide dismutases. *Biol. Chem. 385*, 749–754.
17. Ammendola, S., Pasquali, P., Pacello, F., Rotilio, G., Castor, M., Libby, S., Figueroa-Bossi, N., Bossi, L., Fang, F. C., and Battistoni, A. (2008) Regulatory and structural differences in the Cu,Zn-superoxide dismutase of *Salmonella enterica* and their significance for virulence. *J. Biol. Chem. 283*, 13688–99.
18. Banci, L., Bertini, I., Cramaro, F., Del Conte, R., Rosato, A., and Viezzoli, M. S. (2000) Backbone dynamics of human Cu, Zn superoxide dismustase and of its monomeric F50/EG51E/E133Q mutant: The influence of dimerization on mobility and function. *Biochemistry 39*, 9108–9118.
19. Arnesano, F., Banci, L., and Piccioli, M. (2006) NMR structures of paramagnetic metalloproteins. *Q. Rev. Biophys. 38*, 167–219.
20. Bermel, W., Bertini, I., Felli, I. C., Piccioli, M., and Pierattelli, R. (2006) ^{13}C-Detected *protonless* NMR spectroscopy of proteins in solution. *Prog. NMR Spectrosc. 48*, 25–45.
21. Caillet-Saguy, C., Delepierre, M., Lecroisey, A., Bertini, I., Piccioli, M., and Turano, P. (2006) Direct detected ^{13}C NMR to investigate the iron(III) hemophore HasA. *J. Am. Chem. Soc. 128*, 150–158.
22. Jiménez, B., Mori, M., Battistoni, A., Sette, M., and Piccioli, M. (2007) NMR assignment of reduced form of copper, zinc superoxide dismutase from *Salmonella enterica*. *Biomol. NMR Assignments 1*, 65–68.
23. Cole, R., and Loria, J. P. (2003) FAST-Modelfree: A program for rapid automated analysis of solution NMR spin-relaxation data. *J. Biomol. NMR 26*, 203–213.
24. Dalvit, C. (1996) Homonuclear 1D and 2D NMR experiments for the observation of solvent-solute interactions. *J. Magn. Reson., Ser. B 112*, 282–288.
25. Herrmann, T., Güntert, P., and Wüthrich, K. (2002) Protein NMR structure determination with automated NOE-identification in the NOESY spectra using the new software ATNOS. *J. Biomol. NMR 24*, 171–189.

26. Wishart, D. S., and Sykes, B. D. (1994) The ^{13}C chemical shift index: A simple method for the identification of protein secondary structure using ^{13}C chemical shift data. *J. Biomol. NMR 4*, 171–180.
27. Cordier, F., and Grzesiek, S. (1999) Direct observation of hydrogen bonds in proteins by interresidue $^{3h}J_{NC'}$ scalar couplings. *J. Am. Chem. Soc. 121*, 1601–1602.
28. Banci, L., Bertini, I., Cramaro, F., Del Conte, R., and Viezzoli, M. S. (2002) The solution structure of reduced dimeric copper zinc SOD: The structural effects of dimerization. *Eur. J. Biochem. 269*, 1905–1915.
29. Bertini, I., Duma, L., Felli, I. C., Fey, M., Luchinat, C., Pierattelli, R., and Vasos, P. R. (2004) A heteronuclear direct detection NMR experiment for protein backbone assignment. *Angew. Chem., Int. Ed. 43*, 2257–2259.
30. Bertini, I., Jiménez, B., Piccioli, M., and Poggi, L. (2005) Asymmetry in ^{13}C-^{13}C COSY spectra identifies geometry in paramagnetic proteins. *J. Am. Chem. Soc. 127*, 12216–12217.
31. Balayssac, S., Bertini, I., Luchinat, C., Parigi, G., and Piccioli, M. (2006) ^{13}C direct detected NMR increases the detectability of residual dipolar couplings. *J. Am. Chem. Soc. 128*, 15042–15043.
32. Bermel, W., Bertini, I., Felli, I. C., Lee, Y.-M., Luchinat, C., and Pierattelli, R. (2006) Protonless NMR experiments for sequence-specific assignment of backbone nuclei in unfolded proteins. *J. Am. Chem. Soc. 128*, 3918–3919.
33. Bertini, I., Capozzi, F., Luchinat, C., Piccioli, M., and Viezzoli, M. S. (1991) Assignment of active site protons in the 1H NMR spectrum of reduced human Cu,Zn superoxide dismutase. *Eur. J. Biochem. 197*, 691–697.
34. Folcarelli, S., Battistoni, A., Falconi, M., O'Neill, P., Rotilio, G., and Desideri, A. (1998) Conserved enzyme-substrate electrostatic attraction in prokaryotic Cu,Zn superoxide dismutase. *Biochem. Biophys. Res. Commun. 244*, 908–911.
35. Tainer, J. A., Getzoff, E. D., Beem, K. M., Richardson, J. S., and Richardson, D. C. (1982) Determination and analysis of 2 Å structure of copper zinc superoxide dismutase. *J. Mol. Biol. 160*, 181–217.
36. Djinovic, K., Battistoni, A., Carri, M. T., Polticelli, F., Desideri, A., Rotilio, G., Coda, A., and Bolognesi, M. (1994) Crystal structure of cyanide-inhibited *Xenopus laevis* Cu,Zn superoxide dismutase at 98 K. *FEBS Lett. 349*, 93–98.
37. Battistoni, A., Folcarelli, S., Rotilio, G., Capasso, C., Pesce, A., Bolognesi, M., and Desideri, A. (1996) Crystallization and preliminary X-ray analysis of the monomeric Cu,Zn superoxide dismutase from *Escherichia coli*. *Protein Sci. 5*, 2125–2127.
38. Banci, L., Bertini, I., Cantini, F., D'Onofrio, M., and Viezzoli, M. S. (2002) Structure and dynamics of copper-free SOD: The protein before binding copper. *Protein Sci. 11*, 2479–2492.
39. Djinovic, C. K., Battistoni, A., Carrì, M., Polticelli, F., Desideri, A., Rotilio, G., Coda, A., Wilson, K., and Bolognesi, M. (1996) Three-dimensional structure of *Xenopus laevis* Cu,ZnSOD *b* determined by X-ray crystallogaphy at 1.5 Å resolution. *Acta Crystallogr. D52*, 176–188.
40. Stroppolo, M. E., Nuzzo, S., Pesce, A., Rosano, C., Battistoni, A., Bolognesi, M., Mobilio, S., and Desideri, A. (1998) On the coordination and oxidation states of the active-site copper ion in prokaryotic Cu,Zn superoxide dismutase. *Biochem. Biophys. Res. Commun. 249*, 579–582.
41. Bertini, I., Dalvit, C., Huber, J. G., Luchinat, C., and Piccioli, M. (1997) ePHOGSY experiment on a paramagnetic protein: Location of the catalytic water molecule in the heme crevice of the oxidized form of horse heart cytochrome c. *FEBS Lett. 415*, 45–48.
42. Getzoff, E. D., Cabelli, D. E., Fisher, C. L., Parge, H. E., Viezzoli, M. S., Banci, L., and Hallewell, R. A. (1992) Faster superoxide dismutase mutants designed by enhancing electrostatic guidance. *Nature 358*, 347–351.
43. Falconi, M., Stroppolo, M. E., Cioni, P., Strambini, G., Sergi, A., Ferrario, M., and Desideri, A. (2001) Dynamics-function correlation in Cu,Zn superoxide dismutase: A spectroscopic and molecular duynamics simulation study. *Biophys. J. 80*, 2556–2567.
44. Arnesano, F., Banci, L., Bertini, I., Martinelli, M., Furukawa, Y., and O'Halloran, T. V. (2004) The unusually stable quaternary structure of human SOD1 is controlled by both metal occupancy and disulfide status. *J. Biol. Chem. 279*, 47998–48003.
45. Bertini, I., Luchinat, C., Ming, L.-J., Piccioli, M., Sola, M., and Valentine, J. S. (1992) Two-dimensional ^{1}H-NMR studies of the paramagnetic metalloenzyme copper-nickel superoxide dismutase. *Inorg. Chem. 31*, 4433–4435.
46. Stroppolo, M. E., Pesce, A., D'Orazio, M., O'Neill, P., Bordo, D., Rosano, C., Milani, M., Battistoni, A., Bolognesi, M., and Desideri, A. (2001) Single mutations at the subunit interface modulate copper reactivity in Photobacterium leiognathi Cu,Zn superoxide dismutase. *J. Mol. Biol. 308*, 555–563.
47. Forest, E., Langford, P. R., Kroll, J. S., and Getzoff, E. D. (2000) Cu,Zn superoxide dismutase structure from a microbial pathogen establishes a class with a conserved dimer interface. *J. Mol. Biol. 296*, 145–153.
48. Fang, F. C., DeGroote, M. A., Foster, J. W., Bäumler, A. J., Ochsner, U., Testerman, T., Bearson, S., Giàrd, J. C., Xu, Y., CAmpbell, G., and Laessig, T. (1999) Virulent *Salmonella typhimurium* has two periplasmic Cu, Zn-superoxide dismutases. *Proc. Natl. Acad. Sci. U.S.A. 96*, 7502–7507.
49. Koshunov, S. S., and Imlay, J. A. (2006) Detection and quantification of superoxide formed within the periplasm of *Escherichia coli*. *J. Bacteriol. 188*, 6326–6334.

BI801252E